

See discussions, stats, and author profiles for this publication at: <https://www.researchgate.net/publication/269773355>

Electronic Structure and Optical Signatures of Semiconducting Transition Metal Dichalcogenide Nanosheets

ARTICLE in ACCOUNTS OF CHEMICAL RESEARCH · DECEMBER 2014

Impact Factor: 22.32 · DOI: 10.1021/ar500303m · Source: PubMed

CITATIONS

10

READS

51

3 AUTHORS:



Weijie Zhao

National University of Singapore

22 PUBLICATIONS 739 CITATIONS

[SEE PROFILE](#)



Ricardo Mendes Ribeiro

University of Minho

46 PUBLICATIONS 1,156 CITATIONS

[SEE PROFILE](#)



Goki Eda

National University of Singapore

78 PUBLICATIONS 9,554 CITATIONS

[SEE PROFILE](#)

Electronic Structure and Optical Signatures of Semiconducting Transition Metal Dichalcogenide Nanosheets

Published as part of the Accounts of Chemical Research special issue "2D Nanomaterials beyond Graphene".

Weijie Zhao,^{†,‡} Ricardo Mendes Ribeiro,[§] and Goki Eda^{*,†,‡,||}

[†]Department of Physics, National University of Singapore, 2 Science Drive 3, Singapore 117542

[‡]Graphene Research Centre, National University of Singapore, 6 Science Drive 2, Singapore 117546

[§]Center of Physics and Department of Physics, University of Minho, PT-4710-057, Braga, Portugal

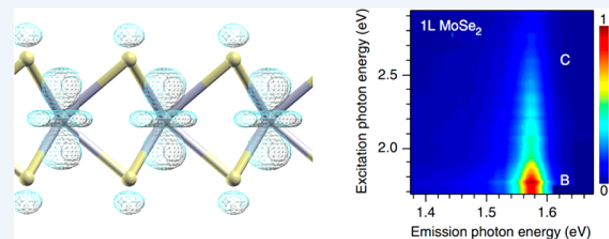
^{||}Department of Chemistry, National University of Singapore, 3 Science Drive 3, Singapore 117543

CONSPECTUS: Two-dimensional (2D) crystals derived from transition metal dichalcogenides (TMDs) are intriguing materials that offer a unique platform to study fundamental physical phenomena as well as to explore development of novel devices. Semiconducting group 6 TMDs such as MoS₂ and WSe₂ are known for their large optical absorption coefficient and their potential for high efficiency photovoltaics and photodetectors. Monolayer sheets of these compounds are flexible, stretchable, and soft semiconductors with a direct band gap in contrast to their well-known bulk crystals that are rigid and hard indirect gap semiconductors. Recent intense research has been motivated by the distinct electrical, optical, and mechanical properties of these TMD crystals in the ultimate thickness regime.

As a semiconductor with a band gap in the visible to near-IR frequencies, these 2D MX₂ materials (M = Mo, W; X = S, Se) exhibit distinct excitonic absorption and emission features. In this Account, we discuss how optical spectroscopy of these materials allows investigation of their electronic properties and the relaxation dynamics of excitons. We first discuss the basic electronic structure of 2D TMDs highlighting the key features of the dispersion relation. With the help of theoretical calculations, we further discuss how photoluminescence energy of direct and indirect excitons provide a guide to understanding the evolution of the electronic structure as a function of the number of layers. We also highlight the behavior of the two competing conduction valleys and their role in the optical processes.

Intercalation of group 6 TMDs by alkali metals results in the structural phase transformation with corresponding semiconductor-to-metal transition. Monolayer TMDs obtained by intercalation-assisted exfoliation retains the metastable metallic phase. Mild annealing, however, destabilizes the metastable phase and gradually restores the original semiconducting phase. Interestingly, the semiconducting 2H phase, metallic 1T phase, and a charge-density-wave-like 1T' phase can coexist within a single crystalline monolayer sheet. We further discuss the electronic properties of the restacked films of chemically exfoliated MoS₂.

Finally, we focus on the strong optical absorption and related exciton relaxation in monolayer and bilayer MX₂. Monolayer MX₂ absorbs as much as 30% of incident photons in the blue region of the visible light despite being atomically thin. This giant absorption is attributed to nesting of the conduction and valence bands, which leads to diversion of optical conductivity. We describe how the relaxation pathway of excitons depends strongly on the excitation energy. Excitation at the band nesting region is of unique significance because it leads to relaxation of electrons and holes with opposite momentum and spontaneous formation of indirect excitons.



INTRODUCTION

The past few years have seen a surge of intense research on two-dimensional (2D) materials based on transition metal dichalcogenides (TMDs).^{1–5} The large family of TMDs sharing a chemical formula of MX₂ (M, transition metal; X, chalcogen) and van der Waals layer structure have been studied in their bulk forms for over half a century for their versatile physical and chemical properties from lubricity to superconductivity.⁶ Studies on ultrathin "2D" crystals of TMDs date back to the initial work on molybdenum disulfide (MoS₂) by Frindt and co-workers in the 1960s.⁷ The recent interest in 2D TMDs was triggered by the observation of direct band gap photoluminescence (PL) from

monolayer MoS₂ by two independent research teams.^{8,9} It is now known that single layers of other group 6 TMDs such as MoSe₂, WS₂, and WSe₂ are similarly luminescent direct gap semiconductors.^{10–12} Their mechanical flexibility, large carrier mobility, unique symmetry, and gate-tunability make these 2D semiconductors attractive as fundamental building blocks for novel optoelectronics and photonics applications.^{2–5}

Special Issue: 2D Nanomaterials beyond Graphene

Received: August 16, 2014

Published: December 17, 2014

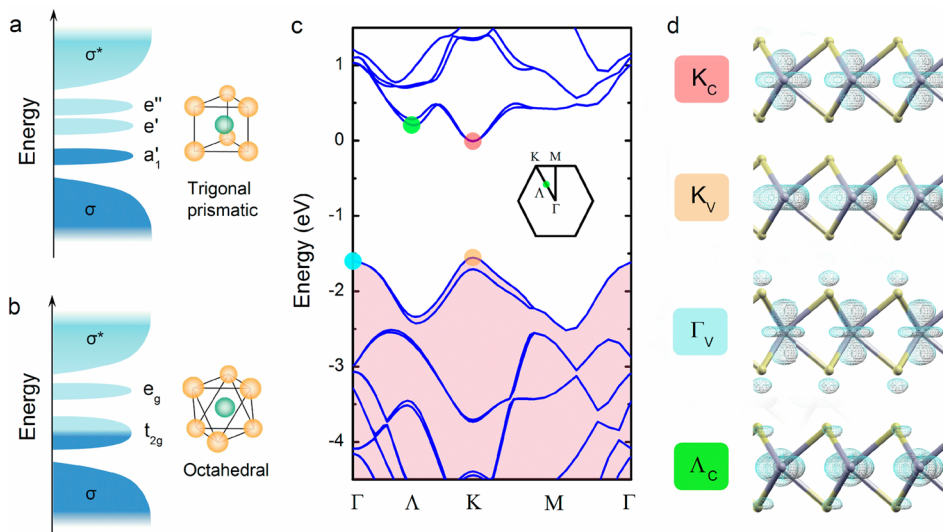


Figure 1. Schematic illustration of orbital filling of group 6 TMDs with trigonal prismatic (a) and octahedral (b) coordination. In trigonal prismatic (2H) coordination, the d orbitals split into three groups, namely, d_z^2 (a_1'), $d_{x^2-y^2,xy}$ (e') and $d_{xz,yz}$ (e''). These orbitals are located within the bonding (σ) and antibonding (σ^*) states. In octahedral (1T) coordination, the d orbitals split into $d_{xy,yz,zx}$ (t_{2g}) and d_{z^2,x^2-y^2} (e_g) bands. (c) Calculated electronic band structure of monolayer MoS₂. (d) Electron distribution for states at the four extrema in the band structure indicated by colored dots in panel c.

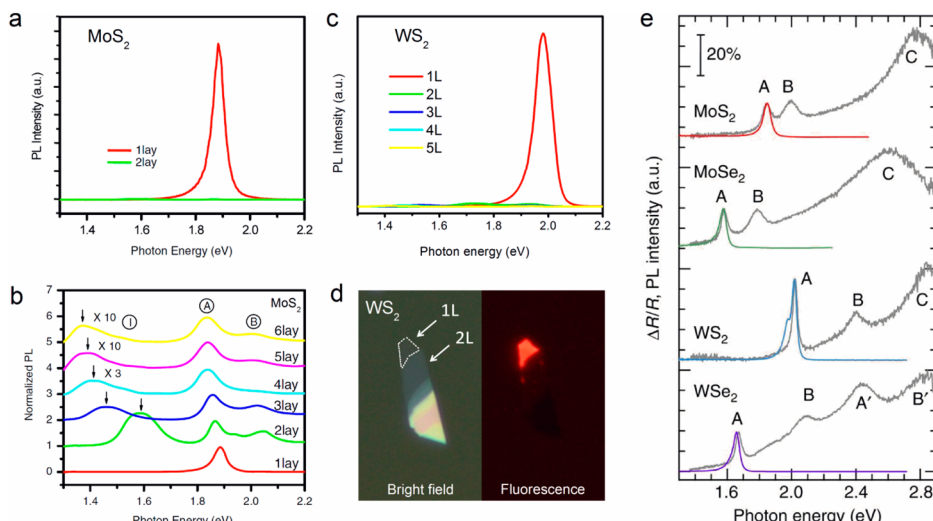


Figure 2. (a) PL spectra of mechanically exfoliated monolayer and bilayer 2H-MoS₂. (b) Normalized PL spectra of 1L–6L MoS₂. The direct gap PL, labeled as A/B, is not sensitive to the number of layers. In contrast, indirect gap emission peak, labeled as I, decreases in energy with increasing number of layers. Adapted with permission from ref 8. Copyright 2010 American Physical Society. (c) PL spectra of 1L–5L WS₂. (d) Bright field optical and fluorescence images of mechanically exfoliated WS₂. The monolayer region shows bright fluorescence compared to other multilayer regions. (e) Normalized PL spectra (colored plots) and differential reflectance spectra (gray plots) of monolayer MX₂ flakes on a quartz substrate. The scale bar indicates 20% absorption based on the differential reflectance spectra. Adapted with permission from ref 56. Macmillan Publishers Ltd. Copyright 2014.

Luminescence of group 6 TMDs occurs in the visible to near-IR frequencies and reveals a great deal of information about their electronic structure,^{8,9} many-body interaction,^{13–15} excited-state coherence,¹⁶ doping,¹⁷ defects,^{18,19} and strain.²⁰ Optical spectroscopy has significantly facilitated the understanding these effects and their interplay. In this Account, we discuss our recent efforts on investigating the electronic properties of 2D group 6 TMDs through optical spectroscopy. This Account is not meant to be a comprehensive review, which are available elsewhere,^{2–5} but is aimed at highlighting some unique features of these 2D materials such as their phase change properties, layer-dependent evolution of electronic structures, and giant optical absorption due to band nesting.

ELECTRONIC STRUCTURE

Many interesting properties of 2D materials arise from the unique dispersion of the electronic states that extend over the 2D plane. Precise description of their electronic structure typically requires rigorous density functional theory (DFT) calculations. The basic electronic properties of TMDs can be, however, predicted from the ligand field splitting of the nonbonding transition metal d-orbitals and the filling of these orbitals.² All layered TMDs crystallize in either octahedral or trigonal prismatic coordination, and the group 6 compounds exhibit the latter in their most stable form (typically referred to as 2H phase). In the 2H phase, the ligand field splitting of the d orbitals leads to the formation of d_z^2 (a_1'), $d_{x^2-y^2,xy}$ (e'), and $d_{xz,yz}$ (e'') bands separated by an energy gap.² The two d electrons of the

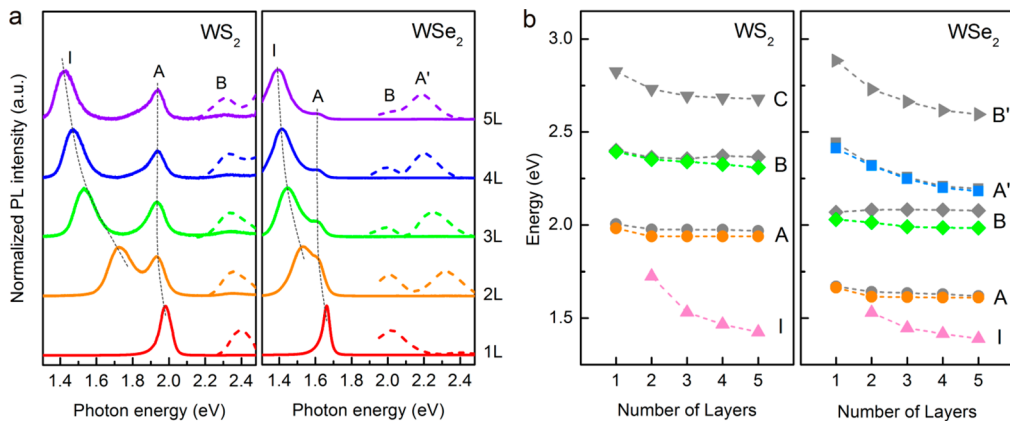


Figure 3. (a) Normalized PL spectra of 1L–SL WS₂ (left) and WSe₂ (right). (b) PL (symbols) and absorption (symbols) peak energies of WS₂ (left) and WSe₂ (right) as a function of the number of layers. The letters I, A, B, A', B', and C refer to the peaks as labeled in Figure 2e and panel a. Adapted with permission from ref 10. Copyright 2013 American Chemical Society.

transition metal fill up the a_1' orbital, making it a semiconductor (Figure 1a). Octahedrally coordinated TMDs (often referred to as 1T phase) form degenerate $d_{xy,yz,zx}$ (t_{2g}) and d_{z^2,x^2-y^2} (e_g) orbitals. Generally, group 6 TMDs are not stable in the octahedral coordination but intercalation by alkali metals^{2,21} and high dose electron irradiation²² are known to induce formation of this phase. Because the lower lying t_{2g} orbital is only partially filled, group 6 TMDs in the 1T phase are metallic in electronic character (Figure 1b). The M–X bonding states (σ) appear deep in the valence band indicating its strong covalent character. The precise position of the M–X antibonding states (σ^*) has been debated,²³ but for clarity it is shown to be above the nonbonding states in Figure 1a,b.

Further understanding of the electronic structure requires consideration of the energy dispersion. Figure 1c shows the DFT calculation of the band structure of monolayer 2H-MoS₂. The key features of the band structure are the two valence band hills and the two conduction band valleys. The valence band hills are at the center (Γ) and corners ($/K'$) of the Brillouin zone. The conduction band valleys are at the K point and the Λ point, which is midway between the $K-\Gamma$ line. Note that the valence band at the K point is split due to spin-orbit coupling. The DFT calculation shows that monolayer MoS₂ is a direct gap semiconductor with the conduction band minimum (CBM) and the valence band maximum (VBM) coinciding at the K point. In contrast, bilayer MoS₂ is an indirect gap semiconductor with CBM at the K point and the VBM at the Γ point (Not shown).

The effect of the number of layers appears most strongly at the conduction band valley at the Λ point (Λ_c) and the valence band hill at the Γ point (Γ_v). Careful examination reveals that the wave function associated with these points consists of an admixture of the metal d orbitals and the chalcogen p_z orbitals. In contrast, the wave functions at the K_c and K_v regions have predominantly d character. The charge density of the p_z orbitals extends to the outer surface of the layer, while the d electrons are confined in the middle of the X–M–X sandwich (Figure 1d).⁹ Thus, the evolution of the band structure results not only from confinement effects but also from the interaction of the chalcogen p_z orbitals of the neighboring layers.

■ PHOTOLUMINESCENCE

Splendiani et al.⁹ and Mak et al.⁸ observed bright PL from monolayer MoS₂ and progressively weaker emission from bilayer

and thicker multilayer samples (Figure 2a), contrary to the expectation that the optical response scales with the volume of the material. The bright PL from monolayer MoS₂ is explained by the efficient recombination of the direct band gap excitons formed at the corners of the Brillouin zone. The emission quantum yield of multilayer MoS₂, which is an indirect gap semiconductor, is negligible because the radiative recombination of indirect excitons is a phonon-assisted second order process and is significantly slower than the nonradiative decay processes.

Multilayer MoS₂ flakes exhibit weak PL with multiple peaks. The lowest energy peak is due to indirect excitons and the higher energy peaks at ~1.9 and 2.05 eV are attributed to hot electron direct gap emission at the K point. The shift of indirect and direct emission energies as a function of the number of layers reveals the evolution of the electronic structure (Figure 2b). We¹⁰ and others^{11,12} have shown that the trend of indirect-to-direct gap crossover is not a unique phenomenon to MoS₂ but is also common to other group 6 TMDs such as MoSe₂, WS₂, and WSe₂, which are isoelectronic to MoS₂ (Figure 2c–e). Note that the electronic gap is larger than the optical gap by exciton binding energy, which has been reported to be of the order of 0.3 eV (ref 24).

■ ABSORPTION

In the near-IR to ultraviolet frequencies, group 6 TMDs exhibit characteristic absorption peaks that can be attributed to excitonic and interband resonances.^{6,8,9} The exciton features are typically dominant and obscure the onset of free carrier absorption.²⁴ The origin of absorption features for bulk crystals have been discussed in several reports including the detailed low temperature studies by Beal and Hughes²⁵ and Bromley et al.²⁶ The A and B exciton resonances arise from optical excitation of electrons from the spin-orbit-split valence band hill to the degenerate conduction band valley at the K point. The C absorption peak, which appears at higher energies (2.6–2.8 eV), has been attributed to band nesting, which leads to a singularity in the joint density of states (JDOS).²⁷ The A' and B' peaks observed in selenides and tellurides have been attributed to splitting of the A and B exciton states. Monolayer crystals typically absorb ~10% of incident photons at their band gap A exciton resonance and more at the C peak resonance (~30%). In comparison to the optical absorption of graphene, which is about 2.3%,²⁸ these large values highlight the unusual light-matter interaction in these monolayer crystals.²⁹

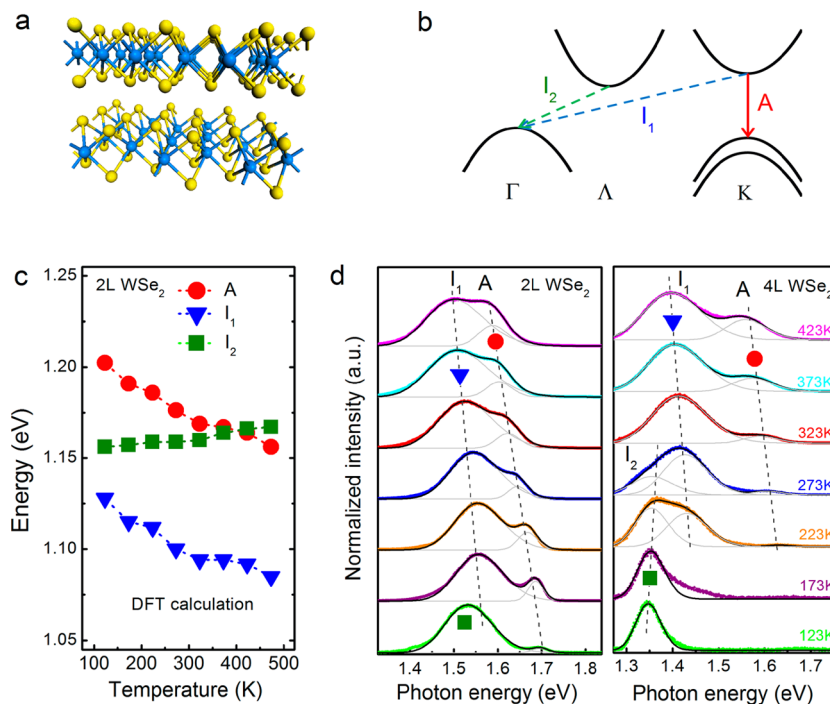


Figure 4. (a) Structure of bilayer 2H-MX₂. (b) Schematic illustration of the band extrema of bilayer 2H-MX₂ and possible radiative relaxation routes for excitons. (c) Calculated direct and indirect transition energies as a function of temperature for bilayer WSe₂. (d) Normalized PL spectra of bilayer (left) and tetralayer (right) WSe₂ measured at different temperatures. The colored plots are the experimental data. The temperature-dependent shift of the direct (A, red circle) and indirect emission peaks (I₁, blue triangle; I₂, green square) are indicated with dashed lines. Panels c and d adapted with permission from ref 41. Copyright 2013 American Chemical Society.

■ WS₂ AND WSe₂

In order to gain insight into the origin of the optical transitions, we investigated the shift of exciton absorption and emission peaks in 1–5 layer (L) WS₂ and WSe₂ (Figure 3a). The number of layers was confirmed by Raman spectroscopy.^{11,30,31} The shift of emission and absorption peaks summarized in Figure 3b clearly indicates that the scaling behavior is unique to each exciton resonance. The A and B exciton energy is only weakly dependent on the crystal thickness, while A', B', and C peak energies increase more rapidly with reduction in the number of layers. The A' and B' excitons in WSe₂, which had been attributed to splitting of the A and B exciton energy levels, show similar trends as the indirect exciton peak. This observation suggests that these optical transitions are more strongly associated with the p_z orbitals of the Se atoms rather than the metal d orbitals.

The confinement-induced change in the band gap of 2D semiconductors (ΔE_g) is predicted to scale as $\Delta E_g = \pi^2 h^2 / (8\mu L_z^2)$ where h is Planck's constant, μ is the reduced mass of the exciton, and L_z is the thickness of the crystals.³² This simple relation does not apply to the optical gap of TMD crystals in the few layer thickness regime for various reasons. First, the band structure of the material is significantly modified with the relative shift of the conduction band valleys and valence band hills. Second, the dielectric properties are correspondingly altered, leading to the remarkable change in the exciton binding energies with layer thickness.³³ Third, extrinsic effects such as unintentional doping by surface adsorbates³⁴ and substrate³⁵ become increasingly important with decreasing thickness and obscure the band gap absorption and emission.

■ CONDUCTION BAND MINIMUM

The band structures obtained from DFT calculations provide a useful guide for identifying the origin of the experimentally observed optical absorption and emission. However, identifying the origin of indirect band gap emission in few-layer MX₂ is a nontrivial task. This is because DFT results show little consensus on the conduction band structure of few-layer MX₂. For bilayer MoS₂ and WS₂, some calculations^{20,33,35–37} show that the CBM is located at the K point while others^{9,36–38} show that it is at the Λ point. On the other hand, the DFT calculations consistently show the VBM to be at the Γ point in few-layer MX₂. The valence band structure has been confirmed to agree with the experimental observations by angle-resolved photoemission spectroscopy.^{39,40}

One fundamental question is whether the CBM in few-layer MX₂ is located at the Λ or K point. Direct investigation of the dispersion of unfilled conduction band states is a challenging task. In order to investigate the relative position of the Λ and K valleys in few-layer MX₂, we studied the temperature dependence of the radiative indirect recombination peak (see schematics in Figure 4a,b).⁴¹

We briefly explain how thermal expansion of the lattice modifies the band structure. The in-plane expansion influences the overlap of the metal d orbitals, which are responsible for the K valleys and hills. Increase in the in-plane lattice constant by Δa leads to reduction of the gap at the K point ($A = E(K_c) - E(K_v)$) and less prominent reduction of the indirect gap between K_c and Γ_v .^{20,42} In contrast, the expansion of interlayer spacing primarily affects the Λ_c and Γ_v points because the p orbital energy of the chalcogen atoms is susceptible to changes in the interlayer coupling. According to the DFT calculations,^{20,42} the Λ valley

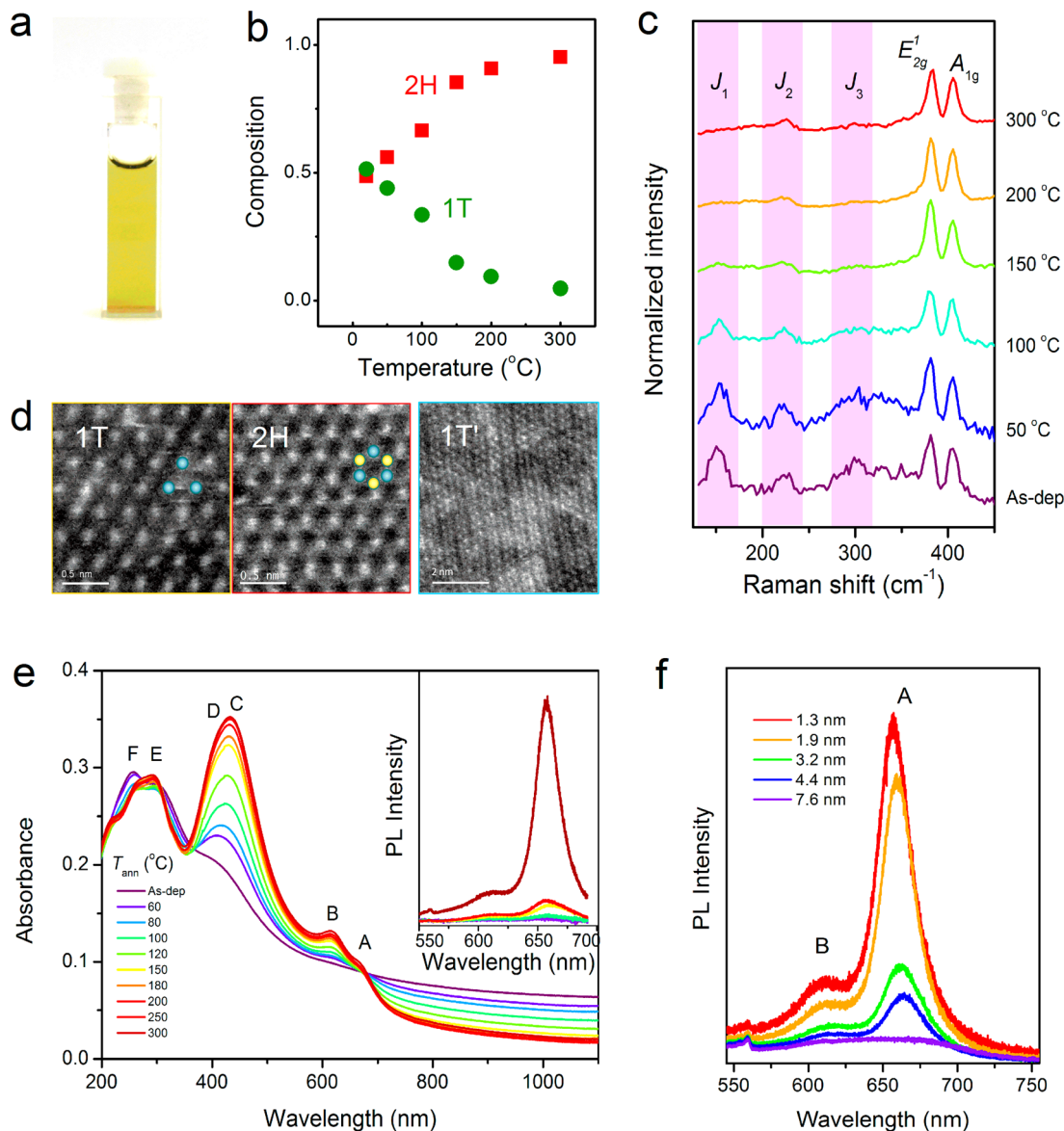


Figure 5. (a) Photograph showing an aqueous suspension of chemically exfoliated MoS₂. (b) Relative composition of 2H and 1T components as a function of annealing temperature obtained from XPS spectra. (c) Raman spectra of chemically exfoliated MoS₂ thin films (~4 nm) annealed at various temperatures. The characteristic Raman peaks for 1T/1T' phase (J₁, J₂, and J₃) are indicated in the shaded regions. (d) High resolution STEM images of 2H, 1T, and 1T' phases. The blue and yellow balls indicate the position of Mo and S atoms. Adapted with permission from ref 53. Copyright 2012 American Chemical Society. (e) Absorption and PL (insert) spectra of MoS₂ thin films with a thickness of ~1.3 nm annealed at various temperatures. (f) PL spectra of MoS₂ thin films with an average thickness ranging from 1.3 to 7.6 nm. Panels a, b, e, and f adapted with permission from ref 51. Copyright 2011 American Chemical Society.

and Γ hill shift upward and downward, respectively, with increasing interlayer expansion.

Thermal expansion of the lattice leads to a composite effect of in-plane and out-of-plane expansion explained above. From the band structure calculated with the temperature-dependent lattice constants for bulk MoS₂ and WSe₂,^{43,44} we found that the two indirect gap energies, $I_1 = E(K_c) - E(\Gamma_v)$ and $I_2 = E(\Lambda_c) - E(\Gamma_v)$, exhibit opposite temperature dependence (Figure 4c). This indicates that the temperature dependence of the indirect gap emission can help us identify whether the Λ or K valley is involved in the transition. Further, by properly taking into account the exciton binding energies, the location of the CBM can be identified.

The temperature coefficient of the indirect emission energy for bilayer WSe₂ was experimentally found to be negative (Figure

4d). This suggests that the indirect optical transition involves the K valley. In contrast, the temperature coefficient in MoS₂ and WS₂ was positive, suggesting that the Λ valley is involved in the optical transition (not shown in figure). Interestingly, thicker few-layer WSe₂ flakes exhibit two indirect emission peaks with opposite temperature coefficients (Figure 4d). These observations indicate that the conduction band valleys in WSe₂ are nearly degenerate as indicated by the DFT results.⁴⁵

■ PHASE TRANSITION

Solution-based exfoliation of layered materials is a promising route to producing 2D crystals in large scale and implementing them into practical applications.^{46–49} Intercalation-assisted or chemical exfoliation is a technique that allows high yield preparation of monolayer TMDs in colloidal suspensions

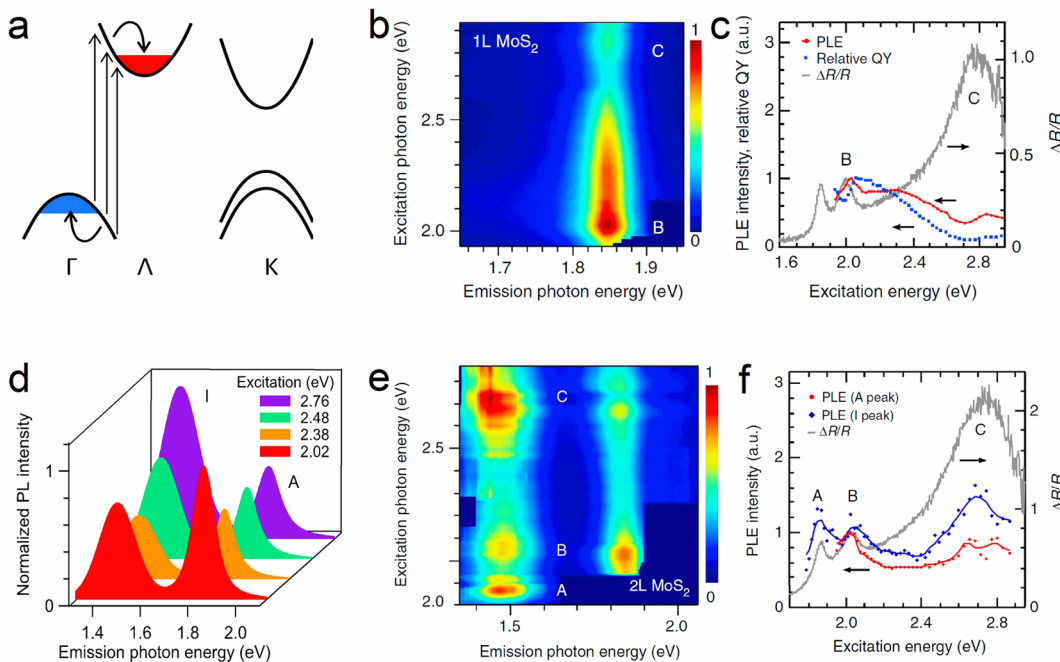


Figure 6. (a) Schematic showing the band extrema of monolayer MX. PLE intensity map (b) and spectrum (c) for band gap emission for monolayer MoS₂. Differential reflectance spectrum is shown for comparison in gray plot. (d) PL spectra of bilayer MoS₂ for different excitation energies. PLE intensity map (e) and spectrum (f) for bilayer MoS₂. Panels b, c, e, and f adapted with permission from ref S6. Macmillan Publishers Ltd. Copyright 2014.

(Figure 5a).⁵⁰ It is well established that alkali metal intercalation of semiconducting 2H-MoS₂ results in its structural transformation to metallic 1T-MoS₂.²¹ Earlier studies have shown that the 1T phase is metastable and converts back to the stable 2H phase upon mild annealing.⁵¹ However, the structure of the exfoliated material and the extent of the restoration of the original 2H phase have been debated.⁵²

X-ray photoelectron spectroscopy (XPS) analyses indicated that the 2H and 1T phases coexist in the as-exfoliated materials at variable fractions.⁵¹ From the XPS results, we determined that the fraction of the 2H phase increases with annealing temperature, reaching 0.95 at 300 °C (Figure 5b). Raman vibrational modes also reveal the gradual loss of 1T phase and recovery of the 2H phase with annealing (Figure 5c).

Atomic resolution scanning transmission electron microscopy (STEM) of chemically exfoliated MoS₂ and WS₂ revealed that the 2H and 1T phases exist in nanoscopic domains within individual sheets.⁵³ Figure 5d shows the annular dark field (ADF) STEM images showing the different contrast variations corresponding to different phases. The charge-density-wave (CDW)-like structure consisting of an anisotropic superlattice of Mo–Mo and W–W zigzag chains^{53,54} is a distorted 1T phase, previously referred to as the 1T' or ZT phase.^{22,55}

The optical absorption spectrum of as-produced chemically exfoliated MoS₂ shows no clear characteristic peaks of pristine 2H-MoS₂ except for the excitonic features in the UV range (200–300 nm). The free-carrier-like broad absorption continuing toward the near-IR region below the optical gap of 2H-MoS₂ reveals the predominantly metallic character of the material. The emergence of the characteristic A, B, and C exciton features of 2H-MoS₂ upon annealing indicates the gradual restoration of the 2H phase (Figure 5e). Characteristic band gap PL features of monolayer 2H-MoS₂ also emerge after mild annealing (Figure 5e, inset). The drop in PL emission intensity and its gradual redshift with increasing film thickness (Figure 5f) are indications of strong interlayer coupling despite the stacking disorder.

BAND NESTING AND PHOTOCARRIER RELAXATION

Despite the atomic thickness, a single layer MX₂ absorbs as much as 30% of incident photons in the blue region of the visible spectrum.⁵⁶ According to DFT calculations,^{27,57} this extraordinary absorption is attributed to the band nesting effect where parallel conduction and valence bands give rise to a singularity feature in the JDOS. The optical conductivity is thus strongly enhanced for energy in resonance with the nesting region of the band structure.

Band nesting has unique implications in the dynamics of photocarrier relaxation. For the resonant excitation condition, the excited electron–hole pairs spontaneously form indirect excitons with electrons and holes relaxing with opposite momentum. The electrons and holes relax toward the Λ_c and Γ_v points, respectively (Figure 6a). In monolayer MX₂, the electrons and holes need to further undergo intervalley scattering to relax to the CBM and VBM at the K point, respectively. Due to the involvement of intervalley phonons, complete thermalization of the photocarriers to the band edge is expected to be slow and inefficient in monolayers. In contrast, Λ_c and Γ_v points are the band extrema in some bilayer MX₂, and photocarrier relaxation to the band edge is expected to be significantly faster.

The photoluminescence excitation (PLE) intensity map of monolayer MoS₂ (Figure 6b) shows that the emission energy is independent of the excitation energy and is consistent with the optical gap. The emission intensity, however, decreases with increasing excitation energy despite increasing absorption. This observation is consistent with the predicted spontaneous formation of indirect excitons with low radiative recombination efficiency.

For bilayer MoS₂, the direct and indirect emission peaks show distinct response to the excitation energy (Figure 6d). The indirect emission (~1.5 eV) intensity is maximized when the excitation is in resonance with the C absorption peak, whereas

the enhancement of the direct emission peak (~ 1.85 eV) at this excitation energy is minor. These behaviors are consistent with the photocarrier dynamics predicted from the band structure and Monte Carlo simulations.⁵⁶

SUMMARY AND OUTLOOK

Optical spectroscopy is an effective approach to probing the essential features of the band structure and many-body effects in 2D TMDs. In particular, the emerging PL from mono- to few-layer MX₂ plays a crucial role in revealing the electronic structure of the material. Theoretical calculations provide a powerful guide to correlating the experimentally observed optical transitions and their shifts to the basic material properties.

Polymorphism of TMDs is a unique characteristic that makes them interesting for various applications from nonvolatile memory devices to electrocatalysis.⁵⁴ Recently observed coexistence of metallic 1T and semiconducting 2H phases along with the highly anisotropic 1T' (or ZT) phase within a single crystalline monolayer flake demonstrates the unusual versatility of these 2D materials. Stabilization of a desired phase and their on-demand formation will potentially enable realization of novel functional nanodevices.

Recent demonstrations of optoelectronic devices based on semiconducting TMDs^{2–5} show positive prospects of these applications. However, the mechanisms responsible for the observed device performance remain largely unexplored. Understanding the transient processes that occur between optical excitation and electrical detection is crucial for identifying the rational device designs and the ideal window of operation. To this end, the unique relaxation dynamics of photocarriers in TMDs can be exploited for hot carrier photovoltaic effects. This requires, for example, intelligent heterostructure design to effectively guide the hot photocarriers to external circuits. van der Waals heterostructures are basic building blocks that could enable manipulation of photocarrier relaxation pathways. Hybridization of the electronic states across van der Waals interfaces predicted by the DFT calculations play a fundamental role in the charge transfer processes.^{58,59} There is currently a gap between the experimental observations and theoretical predictions presumably due to imperfections of experimentally realized heterostructures. Addressing such materials challenges will be key to enabling devices with tailored optoelectronic functionalities.

AUTHOR INFORMATION

Corresponding Author

*E-mail: g.eda@nus.edu.sg.

Author Contributions

The manuscript was written through contributions of all authors. All authors have given approval to the final version of the manuscript.

Funding

G.E. acknowledges Singapore National Research Foundation for funding the research under NRF Research Fellowship (NRF-NRFF2011-02). G.E. also thanks the Graphene Research Centre at the National University of Singapore for funding support. R.M.R is thankful for the financial support by FEDER through the COMPETE Program, by the Portuguese Foundation for Science and Technology (FCT) in the framework of the Strategic Project PEST-C/FIS/UI607/2011 and Grant Nr.

SFRH/BSAB/1249/2012, and by the EC under Graphene Flagship (contract no. CNECT-ICT-604391).

Notes

The authors declare no competing financial interest.

Biographies

Dr. Weijie Zhao received his Ph.D. in 2011 from the Institute of Semiconductors, Chinese Academy of Sciences, Beijing. He joined the National University of Singapore as Research Fellow in 2012. His research interest lies in the electronic and phonon properties of two-dimensional materials.

Dr. Ricardo Mendes Ribeiro received his Ph.D. from the University of Minho. In 2013, he received the Habilitation. He has been Assistant Professor at University of Minho since 1999 and currently is Visiting Associate Professor at the Graphene Research Centre, National University of Singapore. His main research interests are on Theoretical Solid State Physics, specially in two-dimensional materials, like graphene.

Dr. Goki Eda received his M.S. from Worcester Polytechnic Institute and Ph.D. from Rutgers University. He worked at Imperial College London as a Newton International Fellow of the Royal Society of U.K. Dr. Eda joined the National University of Singapore and Graphene Research Centre as Assistant Professor and NRF Research Fellow in 2011.

REFERENCES

- (1) Novoselov, K. S.; Jiang, D.; Schedin, F.; Booth, T. J.; Khotkevich, V. V.; Morozov, S. V.; Geim, A. K. Two-dimensional atomic crystals. *Proc. Natl. Acad. Sci. U.S.A.* **2005**, *102*, 10451–10453.
- (2) Chhowalla, M.; Shin, H. S.; Eda, G.; Li, L.-J.; Loh, K. P.; Zhang, H. The chemistry of two-dimensional layered transition metal dichalcogenide nanosheets. *Nat. Chem.* **2013**, *5*, 263–275.
- (3) Wang, Q. H.; Kalantar-Zadeh, K.; Kis, A.; Coleman, J. N.; Strano, M. S. Electronics and optoelectronics of two-dimensional transition metal dichalcogenides. *Nat. Nanotechnol.* **2012**, *7*, 699–712.
- (4) Geim, A. K.; Grigorieva, I. V. Van der Waals heterostructures. *Nature* **2013**, *499*, 419–425.
- (5) Butler, S. Z.; Hollen, S. M.; Cao, L.; Cui, Y.; Gupta, J. A.; Gutierrez, H. R.; Heinz, T. F.; Hong, S. S.; Huang, J.; Ismach, A. F.; Johnston-Halperin, E.; Kuno, M.; Plashnitsa, V. V.; Robinson, R. D.; Ruoff, R. S.; Salahuddin, S.; Shan, J.; Shi, L.; Spencer, M. G.; Terrones, M.; Windl, W.; Goldberger, J. E. Progress, challenges, and opportunities in two-dimensional materials beyond graphene. *ACS Nano* **2013**, *7*, 2898–2926.
- (6) Wilson, J. A.; Yoffe, A. D. The transition metal dichalcogenides discussion and interpretation of the observed optical, electrical and structural properties. *Adv. Phys.* **1969**, *18*, 193–335.
- (7) Consadori, F.; Frindt, R. F. Crystal size effects on the exciton absorption spectrum of WSe₂. *Phys. Rev. B* **1970**, *2*, 4893–4896.
- (8) Mak, K. F.; Lee, C.; Hone, J.; Shan, J.; Heinz, T. F. Atomically thin MoS₂: A new direct-gap semiconductor. *Phys. Rev. Lett.* **2010**, *105*, No. 136805.
- (9) Splendiani, A.; Sun, L.; Zhang, Y. B.; Li, T. S.; Kim, J.; Chim, C. Y.; Galli, G.; Wang, F. Emerging photoluminescence in monolayer MoS₂. *Nano Lett.* **2010**, *10*, 1271–1275.
- (10) Zhao, W. J.; Ghorannevis, Z.; Chu, L. Q.; Toh, M. L.; Kloc, C.; Tan, P. H.; Eda, G. Evolution of electronic structure in atomically thin sheets of WS₂ and WSe₂. *ACS Nano* **2013**, *7*, 791–797.
- (11) Zeng, H.; Liu, G. B.; Dai, J.; Yan, Y.; Zhu, B.; He, R.; Xie, L.; Xu, S.; Chen, X.; Yao, W.; Cui, X. Optical signature of symmetry variations and spin-valley coupling in atomically thin tungsten dichalcogenides. *Sci. Rep.* **2012**, *3*, 1608.
- (12) Tonndorf, P.; Schmidt, R.; Böttger, P.; Zhang, X.; Börner, J.; Liebig, A.; Albrecht, M.; Kloc, C.; Gordan, O.; Zahn, D. R. T.; Vasconcellos, S. M. D.; Bratschitsch, R. Photoluminescence emission

- and Raman response of monolayer MoS₂, MoSe₂, and WSe₂. *Opt. Express* **2013**, *21*, 4908.
- (13) Mak, K. F.; He, K. L.; Shan, J.; Heinz, T. F. Control of valley polarization in monolayer MoS₂ by optical helicity. *Nat. Nanotechnol.* **2012**, *7*, 494–498.
- (14) Zeng, H. L.; Dai, J. F.; Yao, W.; Xiao, D.; Cui, X. D. Valley polarization in MoS₂ monolayers by optical pumping. *Nat. Nanotechnol.* **2012**, *7*, 490–493.
- (15) Mak, K. F.; He, K. L.; Lee, C.; Lee, G. H.; Hone, J.; Heinz, T. F.; Shan, J. Tightly bound trions in monolayer MoS₂. *Nat. Mater.* **2013**, *12*, 207–211.
- (16) Jones, A. M.; Yu, H. Y.; Ghimire, N.; Wu, S. F.; Aivazian, G.; Ross, J. S.; Zhao, B.; Yan, J. Q.; Mandrus, D.; Xiao, D.; Yao, W.; Xu, X. D. Optical Generation of Excitonic Valley Coherence in Monolayer WSe₂. *Nat. Nanotechnol.* **2013**, *8*, 634–638.
- (17) Radisavljevic, B.; Kis, A. Mobility engineering and a metal-insulator transition in monolayer MoS₂. *Nat. Mater.* **2013**, *12*, 815–820.
- (18) Ye, J. T.; Zhang, Y. J.; Akashi, R.; Bahramy, M. S.; Arita, R.; Iwasa, Y. Superconducting dome in a gate-tuned band insulator. *Science* **2012**, *338*, 1193–1196.
- (19) Najmaei, S.; Liu, Z.; Zhou, W.; Zou, X.; Shi, G.; Lei, S.; Yakobson, B. I.; Idrobo, J. C.; Ajayan, P. M.; Lou, J. Vapour phase growth and grain boundary structure of molybdenum disulphide atomic layers. *Nat. Mater.* **2013**, *12*, 754–759.
- (20) Feng, J.; Qian, X. F.; Huang, C. W.; Li, J. Strain-engineered artificial atom as a broad-spectrum solar energy funnel. *Nat. Photonics* **2012**, *6*, 865–871.
- (21) Py, M. A.; Haering, R. R. Structural destabilization induced by lithium intercalation in MoS₂ and related compounds. *Can. J. Phys.* **1983**, *61*, 76–84.
- (22) Lin, Y. C.; Dumcenco, D. O.; Huang, Y. S.; Suenaga, K. Atomic mechanism of the semiconducting-to-metallic phase transition in single-layered MoS₂. *Nat. Nanotechnol.* **2014**, *9*, 391–396.
- (23) Coehoorn, R.; Haas, C.; de Groot, R. A. Electronic structure of MoSe₂, MoS₂, and WSe₂. II. The nature of the optical band gaps. *Phys. Rev. B* **1987**, *35*, 6203–6206.
- (24) Chernikov, A.; Berkelbach, T. C.; Hill, H. M.; Rigosi, A.; Li, Y.; Aslan, O. B.; Reichman, D. R.; Hybertsen, M. S.; Heinz, T. F. Exciton Binding Energy and Nonhydrogenic Rydberg Series in Monolayer WS₂. *Phys. Rev. Lett.* **2014**, *113*, No. 076802.
- (25) Beal, A. R.; Hughes, H. P. Kramers-Kronig analysis of the reflectivity spectra of 2H-MoS₂, 2H-MoSe₂ and 2H-MoTe₂. *J. Phys. C: Solid State Phys.* **1979**, *12*, 881.
- (26) Bromley, R. A.; Murray, R. B.; Yoffe, A. D. The band structures of some transition metal dichalcogenides. III. Group VIA: trigonal prism materials. *J. Phys. C: Solid State Phys.* **1972**, *5*, 759.
- (27) Carvalho, A.; Ribeiro, R. M.; Castro Neto, A. H. Band nesting and the optical response of two-dimensional semiconducting transition metal dichalcogenides. *Phys. Rev. B* **2013**, *88*, No. 115205.
- (28) Nair, R. R.; Blake, P.; Grigorenko, A. N.; Novoselov, K. S.; Booth, T. J.; Stauber, T.; Peres, N. M.; Geim, A. K. Fine structure constant defines visual transparency of graphene. *Science* **2008**, *320*, 1308.
- (29) Britnell, L.; Ribeiro, R. M.; Eckmann, A.; Jalil, R.; Belle, B. D.; Mishchenko, A.; Kim, Y.-J.; Gorbachev, R. V.; Georgiou, T.; Morozov, S. V.; Grigorenko, A. N.; Geim, A. K.; Casiraghi, C.; Neto, A. H. C.; Novoselov, K. S. Strong Light-Matter Interactions in Heterostructures of Atomically Thin Films. *Science* **2013**, *340*, 1311–1314.
- (30) Lee, C.; Yan, H.; Brus, L. E.; Heinz, T. F.; Hone, J.; Ryu, S. Anomalous Lattice Vibrations of Single- and Few-Layer MoS₂. *ACS Nano* **2010**, *4*, 2695–2700.
- (31) Zhao, W. J.; Ghorannevis, Z.; Kumar, A. K.; Pang, J. R.; Toh, M. L.; Zhang, X.; Kloc, C.; Tan, P. H.; Eda, G. Lattice dynamics in mono- and few-layer sheets of WS₂ and WSe₂. *Nanoscale* **2013**, *5*, 9677–9683.
- (32) Yoffe, A. D. Low-dimensional systems: Quantum size effects and electronic properties of semiconductor microcrystallites (zero-dimensional systems) and some quasi-two-dimensional systems. *Adv. Phys.* **2002**, *51*, 799–890.
- (33) Cheiwchanchamnangij, T.; Lambrecht, W. R. L. Quasiparticle band structure calculation of monolayer, bilayer, and bulk MoS₂. *Phys. Rev. B* **2012**, *85*, No. 205302.
- (34) Tongay, S.; Zhou, J.; Ataca, C.; Liu, J.; Kang, J. S.; Matthews, T. S.; You, L.; Li, J.; Grossman, J. C.; Wu, J. Broad-range modulation of light emission in two-dimensional semiconductors by molecular physisorption gating. *Nano Lett.* **2013**, *13*, 2831–2836.
- (35) Komsa, H. P.; Krasheninnikov, A. V. Effects of confinement and environment on the electronic structure and exciton binding energy of MoS₂ from first principles. *Phys. Rev. B* **2012**, *86*, No. 241201.
- (36) Yun, W. S.; Han, S. W.; Hong, S. C.; Kim, I. G.; Lee, J. D. Thickness and strain effects on electronic structures of transition metal dichalcogenides: 2H-MX₂ semiconductors (M = Mo, W; X = S, Se, Te). *Phys. Rev. B* **2012**, *85*, No. 033305.
- (37) Kuc, A.; Zibouche, N.; Heine, T. Influence of quantum confinement on the electronic structure of the transition metal sulfide TS₂. *Phys. Rev. B* **2011**, *83*, No. 245213.
- (38) Ramasubramaniam, A.; Naveh, D.; Towe, E. Tunable band gaps in bilayer transition-metal dichalcogenides. *Phys. Rev. B* **2011**, *84*, No. 205325.
- (39) Jin, W.; Yeh, P.-C.; Zaki, N.; Zhang, D.; Sadowski, J. T.; Al-Mahboob, A.; van der Zande, A. M.; Chenet, D. A.; Dadap, J. I.; Herman, I. P.; Sutter, P.; Hone, J.; Osgood, R. M., Jr. Direct Measurement of the Thickness-Dependent Electronic Band Structure of MoS₂ Using Angle-Resolved Photoemission Spectroscopy. *Phys. Rev. Lett.* **2013**, *111*, No. 106801.
- (40) Klein, A.; Tiefenbacher, S.; Eyert, V.; Pettenkofer, C.; Jaegermann, W. Electronic band structure of single-crystal and single-layer WS₂: Influence of interlayer van der Waals interactions. *Phys. Rev. B* **2001**, *64*, No. 205416.
- (41) Zhao, W.; Ribeiro, R. M.; Toh, M.; Carvalho, A.; Kloc, C.; Castro Neto, A. H.; Eda, G. Origin of indirect optical transitions in few-layer MoS₂, WS₂, and WSe₂. *Nano Lett.* **2013**, *13*, 5627–5634.
- (42) Peelaers, H.; Van de Walle, C. G. Effects of strain on band structure and effective masses in MoS₂. *Phys. Rev. B* **2012**, *86*, No. 241401.
- (43) El-Mahalawy, S. H.; Evans, B. L. The thermal expansion of 2H-MoS₂, 2H-MoSe₂ and 2H-WSe₂ between 20 and 800°C. *J. Appl. Crystallogr.* **1976**, *9*, 403–406.
- (44) Murray, R.; Evans, B. L. The thermal expansion of 2H-MoS₂ and 2H-WSe₂ between 10 and 320 K. *J. Appl. Crystallogr.* **1979**, *12*, 312–315.
- (45) Sahin, H.; Tongay, S.; Horzum, S.; Fan, W.; Zhou, J.; Li, J.; Wu, J.; Peeters, F. M. Anomalous Raman spectra and thickness-dependent electronic properties of WSe₂. *Phys. Rev. B* **2013**, *87*, No. 165409.
- (46) Eda, G.; Chhowalla, M. Chemically derived graphene oxide: Towards large-area thin-film electronics and optoelectronics. *Adv. Mater.* **2010**, *22*, 2392–2415.
- (47) Coleman, J. N.; Lotya, M.; O'Neill, A.; Bergin, S. D.; King, P. J.; Khan, U.; Young, K.; Gaucher, A.; De, S.; Smith, R. J.; Shvets, I. V.; Arora, S. K.; Stanton, G.; Kim, H. Y.; Lee, K.; Kim, G. T.; Duesberg, G. S.; Hallam, T.; Boland, J. J.; Wang, J. J.; Donegan, J. F.; Grunlan, J. C.; Moriarty, G.; Shmeliov, A.; Nicholls, R. J.; Perkins, J. M.; Grieveson, E. M.; Theuwissen, K.; McComb, D. W.; Nellist, P. D.; Nicolosi, V. Two-dimensional nanosheets produced by liquid exfoliation of layered materials. *Science* **2011**, *331*, 568–571.
- (48) Nicolosi, V.; Chhowalla, M.; Kanatzidis, M. G.; Strano, M. S.; Coleman, J. N. Liquid exfoliation of layered materials. *Science* **2013**, *340*, No. 1226419.
- (49) King, L. A.; Zhao, W.; Chhowalla, M.; Riley, D. J.; Eda, G. Photoelectrochemical properties of chemically exfoliated MoS₂. *J. Mater. Chem. A* **2013**, *1*, 8935–8941.
- (50) Joensen, P.; Crozier, E. D.; Alberding, N.; Frindt, R. F. A study of single-layer and restacked MoS₂ by X-ray diffraction and X-ray absorption spectroscopy. *J. Phys. C: Solid State Phys.* **1987**, *20*, 4043.
- (51) Eda, G.; Yamaguchi, H.; Voiry, D.; Fujita, T.; Chen, M.; Chhowalla, M. Photoluminescence from chemically exfoliated MoS₂. *Nano Lett.* **2011**, *11*, 5111–5116.

- (52) Heising, J.; Kanatzidis, M. G. Structure of restacked MoS₂ and WS₂ elucidated by electron crystallography. *J. Am. Chem. Soc.* **1999**, *121*, 638–643.
- (53) Eda, G.; Fujita, T.; Yamaguchi, H.; Voiry, D.; Chen, M.; Chhowalla, M. Coherent atomic and electronic heterostructures of single-layer MoS₂. *ACS Nano* **2012**, *6*, 7311–7317.
- (54) Voiry, D.; Yamaguchi, H.; Li, J.; Silva, R.; Alves, D. C. B.; Fujita, T.; Chen, M.; Asefa, T.; Shenoy, V. B.; Eda, G.; Chhowalla, M. Enhanced catalytic activity in strained chemically exfoliated WS₂ nanosheets for hydrogen evolution. *Nat. Mater.* **2013**, *12*, 850–855.
- (55) Kan, M.; Wang, J. Y.; Li, X. W.; Zhang, S. H.; Li, Y. W.; Kawazoe, Y.; Sun, Q.; Jena, P. Structures and phase transition of a MoS₂ monolayer. *J. Phys. Chem. C* **2014**, *118*, 1515–1522.
- (56) Kozawa, D.; Kumar, R.; Carvalho, A.; Kumar Amara, K.; Zhao, W.; Wang, S.; Toh, M.; Ribeiro, R. M.; Castro Neto, A. H.; Matsuda, K.; Eda, G. Photocarrier relaxation pathway in two-dimensional semiconducting transition metal dichalcogenides. *Nat. Commun.* **2014**, *5*, No. 4543.
- (57) Qiu, D. Y.; da Jornada, F. H.; Louie, S. G. Optical spectrum of MoS₂: Many-body effects and diversity of exciton states. *Phys. Rev. Lett.* **2013**, *111*, No. 216805.
- (58) Kośmider, K.; Fernández-Rossier, J. Electronic properties of the MoS₂-WS₂ heterojunction. *Phys. Rev. B* **2013**, *87*, No. 075451.
- (59) Terrones, H.; Lopez-Urias, F.; Terrones, M. Novel hetero-layered materials with tunable direct band gaps by sandwiching different metal disulfides and diselenides. *Sci. Rep.* **2013**, *3*, No. 1549.